J Neurophysiol 90: 1598–1612, 2003.
First published May 15, 2003; 10.1152/jn.00293.2003.

Neocortical Pyramidal Cells Respond as Integrate-and-Fire Neurons to In Vivo–Like Input Currents

Alexander Rauch,* Giancarlo La Camera,* Hans-Rudolf Lüscher, Walter Senn, and Stefano Fusi
Institute of Physiology, University of Bern, 3012 Bern, Switzerland

Submitted 26 March 2003; accepted in final form 7 May 2003

Rauch, Alexander, Giancarlo La Camera, Hans-Rudolf Lüscher, Walter Senn, and Stefano Fusi. Neocortical pyramidal cells respond as integrate-and-fire neurons to in vivo–like input currents. *J Neurophysiol* 90: 1598–1612, 2003. First published May 15, 2003; 10.1152/jn.00293.2003. In the intact brain neurons are constantly exposed to intense synaptic activity. This heavy barrage of excitatory and inhibitory inputs was recreated in vitro by injecting a noisy current, generated as an Ornstein–Uhlenbeck process, into the soma of rat neocortical pyramidal cells. The response to such in vivo–like currents was studied systematically by analyzing the time development of the instantaneous spike frequency, and when possible, the stationary mean spike frequency as a function of both the mean and the variance of the input current. All cells responded with an in vivo–like action potential activity with stationary statistics that could be sustained throughout long stimulation intervals (tens of seconds), provided the frequencies were not too high. The temporal evolution of the response revealed the presence of mechanisms of fast and slow spike frequency adaptation, and a medium duration mechanism of facilitation. For strong input currents, the slow adaptation mechanism made the spike frequency response nonstationary. The minimal frequencies that caused strong slow adaptation (a decrease in the spike rate by more than 1 Hz/s), were in the range 30–80 Hz and depended on the pipette solution used. The stationary response function has been fitted by two simple models of integrate-and-fire neurons endowed with a frequency-dependent modification of the input current. This accounts for all the fast and slow mechanisms of adaptation and facilitation that determine the stationary response, and proved necessary to fit the model to the experimental data. The coefficient of variability of the interspike interval was also in part captured by the model neurons, by tuning the parameters of the model to match the mean spike frequencies only. We conclude that the integrate-and-fire model with spike-frequency–dependent adaptation/facilitation is an adequate model reduction of cortical cells when the mean spike-frequency response to in vivo–like currents with stationary statistics is considered.

INTRODUCTION

Single neuron properties have been thoroughly investigated in the past years showing that neural cells are rich in phenomenology and complex in their structure (see, e.g., Mainen and Sejnowski 1996; McCormick et al. 1985; Rhodes 1999). Even the most detailed state-of-the-art model is unable to capture the entire phenomenology observed in the experiments. Such a richness calls for a model reduction that could provide a synthetic description of the response properties of the cells under particular conditions. We studied in vitro those features that are supposedly relevant when the cell is embedded in a large network of interconnected neurons, as it would be in in vivo conditions. The guidelines for selecting the relevant features were dictated by the theoretical framework developed in the last decade to study the dynamic properties of networks of integrate-and-fire neurons (see Gerstner and Kistler 2002 for a review). This approach was already successful in relating single neuron properties to several in vivo phenomena (Amit and Tsodyks 1991; Brunel 2000b) like the omnipresent spontaneous activity (Amit and Brunel 1997) or the persistent, selective delay activity observed in many areas of the cortex in behaving animals (Amit and Brunel 1997; Wang 2001; Yakovlev et al. 1998). In both cases the recorded spike activity is sustained throughout long intervals: low, spontaneous activity is always present, whereas elevated delay activity can last $\leq$30s (Fuster 1995). During these intervals the statistics of the total synaptic input are likely to be stationary or quasi-stationary, that is, to vary on time scales that are much longer than the "reaction" time (Gerstner and Kistler 2002) of the assembly of neurons.

Despite the steadiness of the statistics, the total synaptic current results from a considerably irregular synaptic activity, and hence fluctuates all the time. Neurons on the presynaptic side emit spikes spontaneously at a frequency of a few spikes s^{-1} and the neocortical connectivity is rather high [approximately 10^4 synapses per neuron (Abeles 1991)]. As a consequence, during the interval between two successive spikes, every neuron integrates hundreds of excitatory and inhibitory postsynaptic potentials that arrive at random times. If the spike activities of the presynaptic neurons are statistically independent (see METHODS) then the resulting total synaptic conductance can be described as a random walk with a Gaussian distribution and finite time correlation length determined by the time development of unitary synaptic events [an Ornstein–Uhlenbeck process (Tuckwell 1988)]. Interestingly in vitro neocortical neurons produce in vivo–like activity when noisy current waveforms are injected (Destexhe et al. 2001; Mainen and Sejnowski 1995), and there is some preliminary indirect evidence, based on the analysis of the distribution of the membrane potential recorded intracellularly in vivo, that somatic currents could be modeled as an Ornstein–Uhlenbeck process (Destexhe and Paré 1999, 2000). The total synaptic current is also approximately Gaussian (Amit and Tsodyks 1992) (also see DISCUSSION and the APPENDIX) and, for fast synaptic currents (AMPA or $GABA_A$), the time correlation

*A. Rauch and G. La Camera contributed equally to this work.

Address for reprint requests: S. Fusi, Institute of Physiology, University of Bern, Bühlplatz 5, 3012 Bern, Switzerland (E-mail: fusi@cns.unibe.ch).

The costs of publication of this article were defrayed in part by the payment of page charges. The article must therefore be hereby marked "*advertisement*" in accordance with 18 U.S.C. Section 1734 solely to indicate this fact.

length is short compared with other inherent time constants of the neuron (e.g., the membrane time constant). As a consequence the total input current is practically white noise and can be fully characterized by its average m_I and SD s_I.

In the present work we measured the response function of neocortical pyramidal cells to such a noisy current with stationary statistics. We first studied the time development of the neuronal response and characterized the functional role of the adaptation/facilitation components that determine the statistical properties of stationary responses. These components act on different time scales and, for some input currents, reach a steady regime in which they either disappear or are combined together to determine the stationary statistics of the train of spikes generated by the neuron. We then analyzed quantitatively the stationary responses by exploring systematically the whole parameter space $\{m_I, s_I\}$ characterizing the input current and determining the resulting spike frequency f. The measured frequencies have been fitted by the theoretical response functions of two simple models of integrate-and-fire neurons with a single, effective component of adaptation/facilitation. These response functions have been computed analytically (Fusi and Mattia 1999; Ricciardi 1977) and have a relatively simple form. The value of this data modeling is multiple: besides providing a synthetic and efficient way of describing the whole data set, it allows reliable prediction of the output rate in response to currents not used in the experiment and, hence, to cover a wide class of experiments that study the response of the neuron when moving along some specific trajectory in the parameter space of the input current (see e.g., Chance et al. 2002). Moreover, the choice of the response function of model neurons instead of an arbitrary function gives a direct interpretation of the estimated parameters: they are the *effective* parameters of a model neuron that can re-create the measured response of pyramidal cells. The knowledge of these parameters also allows one to make quantitative predictions about the global dynamics of a network (in vivo) of this kind of cells. In addition, the response function to inputs with stationary statistics also gives important information about the reaction time of the network (Fourcaud and Brunel 2002; Gerstner and Kistler 2002; Mattia and DelGiudice 2002). If the parameters are tuned to reproduce the mean spike frequencies, the simulated neurons can also re-create the higher-order statistics of the interspike intervals expressing, for instance, the degree of irregularity of the spike train (e.g., the coefficient of variability of the interspike intervals). Finally, the statistics of the effective parameters across different cells provide a quantitative estimate of the heterogeneity of the functional properties of the cells.

METHODS

Experimental preparation and recordings

Parasagittal slices of rat somatosensory cortex (300 μm thick) were prepared from 15- to 40-day-old female and male Wistar rats according to the institutional guidelines. The preparation was done in ice-cold extracellular solution using a Campden vibratome (752M; Campden Instruments, Loughborough, UK). Slices were incubated at 35°C for 25 min and afterward left at room temperature until being transferred to the recording chamber. The cells were visualized by infrared differential interference contrast videomicroscopy using a Newvicon camera (C2400, Hamamatsu City, Japan) and an infrared filter (RG9, Schott Mainz, Germany) mounted on an upright microscope (Axioscope FS, Zeiss, Germany).

We recorded in current-clamp whole cell configuration from the soma of layer 5 regular spiking (McCormick et al. 1985) pyramidal cells. Recordings and stimulations were made with an Axoclamp-2A amplifier (Axon Instruments, Burlingame, CA) in combination with Clampex 8 (Axon Instruments). The access resistance and the capacitance were compensated using the bridge balance and the capacitance neutralization after having established the whole cell configuration. The data were low-pass filtered at 2.5 kHz with sampling frequency twice the filter frequency. The temperature of the external solution was 31°C. Neurons were visually identified and some of them were filled with biocytin and then stained according to the avidin–biotin–peroxidase (ABC) procedure (Hsu et al. 1981).

Slices were continuously superfused with an artificial cerebrospinal fluid containing (in mM): 125 NaCl, 25 $NaHCO_3$, 2.5 KCl, 1.25 NaH_2PO_4, 2 $CaCl_2$, 1 $MgCl_2$, 25 glucose, gassed with 95% O_2-5% CO_2.

The pipette solution for most of the analyzed cells contained (in mM): 110 K-gluconate, 30 KCl, 10 EGTA, 10 HEPES, 4 Mg-ATP, 0.3 Na_2-GTP, 10 Na_2-phosphocreatine, pH adjusted to 7.3 with KOH. This solution contains a relatively high concentration of EGTA, which allowed long stable recordings and made the cells produce more consistent responses (see *Stimulation protocol and observables*). We tried to identify undesired artifacts introduced by EGTA by studying the cell's response when two other pipette solutions were used. In what follows we will refer to the solution with high concentration of EGTA as the EGTA pipette solution. The other two pipette solutions were labeled $KMeSO_4$ and KGluc and contained (in mM): $KMeSO_4$: 135 K-methylsulfate, 20 KCl, 0.08 EGTA, 0.045 $CaCl_2$, 10 HEPES, 4 Mg-ATP, 0.3 Na_2-GTP, 10 Na_2-phosphocreatine, pH adjusted to 7.3 with KOH. KGluc: 115 K-gluconate, 20 KCl, 10 HEPES, 4 Mg-ATP, 0.3 Na_2-GTP, 10 Na_2-phosphocreatine, pH adjusted to 7.3 with KOH. Pipette solution KGluc was always used with 10 mM biocytin. The measured osmolarity of all three pipette solutions was between 310 and 325 mOsm. Because pyramidal cells of the somatosensory cortex in vitro showed virtually no spontaneous activity, we did not systematically block synaptic input mediated by ligand-gated channels. Control experiments with blocked synaptic inputs by adding 50 μM D-APV, 10 μM CNQX, and 10 μM bicuculline to the extracellular solution did not change the spike frequency.

The input resistance of the neurons was calculated from the voltage transients in response to at least three different hyperpolarizing (600-ms duration, average of the last 300 ms) current pulses (amplitude, 0.05 nA). The membrane time constant τ_m was estimated by injecting brief (0.5 ms) hyperpolarizing current pulses (-2.5 nA) into the soma. From the decaying averaged ($n = 50$) voltage transient after this current pulse, τ_m was obtained from the slope of a straight line fitted through the tail portion of the semilogarithmic plot of the membrane voltage against time (Iansek and Redman 1973).

Model of in vivo–like input current

We assume that a large number of presynaptic neurons emit spikes at random times. On the postsynaptic side this heavy barrage is felt as a total synaptic current I that evolves as a random walk. If the synaptic currents are summed linearly and the different inputs are statistically independent (i.e., the emission of a spike by one presynaptic neuron does not affect or only slightly affects the initiation of an action potential in another presynaptic neuron) then the random walk can be replaced by a smoother version, the Ornstein–Uhlenbeck process (Tuckwell 1988), characterized by a Gaussian distribution (mean m_I, SD s_I) and by a time-correlation length τ_I. If the synaptic evoked potentials sum linearly and there are N_e excitatory AMPA receptors, each activated at a mean rate f_e and N_i inhibitory $GABA_A$ receptors (f_i), then

$$m_I = N_e \bar{I}_e f_e \tau_I - N_i \bar{I}_i f_i \tau_I \quad (1)$$

$$s_I^2 = \tfrac{1}{2} N_e \bar{I}_e^2 f_e \tau_I + \tfrac{1}{2} N_i \bar{I}_i^2 f_i \tau_I \quad (2)$$

For simplicity we assumed that the time courses of AMPA and $GABA_A$ receptors are the same ($\tau_{ampa} = \tau_{gaba} = \tau_I$). $\bar{I}_e$ ($\bar{I}_i$) is the average peak postsynaptic current evoked by the arrival of a single excitatory (inhibitory) spike. The rise time to this peak current is zero, and then the current decays exponentially: $I(t) = \bar{I}_{e,i} e^{-t/\tau_1}$. (See the APPENDIX for more details on how these constants are related to the mean synaptic conductances.) Slow NMDA components can be added to m_I only, given that they leave s_I almost unaffected (Brunel and Wang 2001). The total synaptic current $I(t)$ can be generated with a single equation

$$dI = -\frac{I(t)}{\tau_I} dt + \mu_I dt + \sigma_I \sqrt{dt}\, \xi(t) \quad (3)$$

which is what was used in the experiment ($\mu_I = m_I/\tau_I$, $\sigma_I^2 = 2s_I^2/\tau_1$).

Stimulation protocol and observables

The noisy input current was generated as an Ornstein–Uhlenbeck stochastic process by iterating the following expression

$$I(t + \Delta t) = I(t) - \frac{I(t)}{\tau_I} \Delta t + \mu_I \Delta t + \sigma_I \xi(t) \sqrt{\Delta t} \quad (4)$$

where ξ_t is a unitary Gauss distributed random variable, updated at every time step. The process was generated and injected at a rate of 5 kHz ($\Delta t = 0.2$ ms) and the correlation length τ_I was usually 1 ms (for 10 cells we also used $\tau_I = 5$ ms). The resulting current $I(t)$ has a stationary Gauss distribution with mean $m_I = \mu_I \tau_I$ and variance $s_I^2 = \sigma_I^2 \tau_1/2$ (Cox and Miller 1965).

The space $\{m_I, s_I\}$ was systematically explored as follows: data points were collected at fixed s_I (ranging from 0 to 500 pA), stepwise increasing m_I from a subthreshold value up to nonstationary frequencies. This protocol was used to determine the threshold mean current (the rheobase current). Then, the whole space $\{m_I, s_I\}$ was discretized and then explored in random order to prevent correlations between time and one of the two parameters m_I, s_I. In both protocols, the duration of the stimulation depended on the cell response: it was 10 s long, or shorter if ≥150 spikes were collected. For those cells used to characterize the response over time (see RESULTS), a stimulus duration of 10 s was always used. The first transient part of the neuronal response (2 s if the stimulation time was longer than 4 s; 0.5 s otherwise) was discarded when estimating the mean spike frequency and the coefficient of variability (see following text). The intervals between successive stimulations were 50–60 s (Fig. 1).

The mean spike frequency (response) was estimated as the ratio between the total number of action potentials N_{sp} and the stimulus duration T. The confidence intervals (68%) of the experimentally measured frequencies were given by $\Delta = (\Delta f^+ + \Delta f^-)/2$, with (see, e.g., Meyer 1965)

$$\Delta f^{\pm} = \frac{1}{T} \left| \frac{1}{2} \pm \sqrt{N_{sp} + \frac{1}{4}} \right| \quad (5)$$

The coefficient of variability (CV) of the interspike interval was estimated as the ratio between the SD and the mean of the interspike intervals.

Particular care was taken to ensure that the response of the cell was consistent throughout the whole recording session. Usually the cells showed a transient phase at the beginning, followed by a long time interval (10–90 min) during which the response was consistent (when

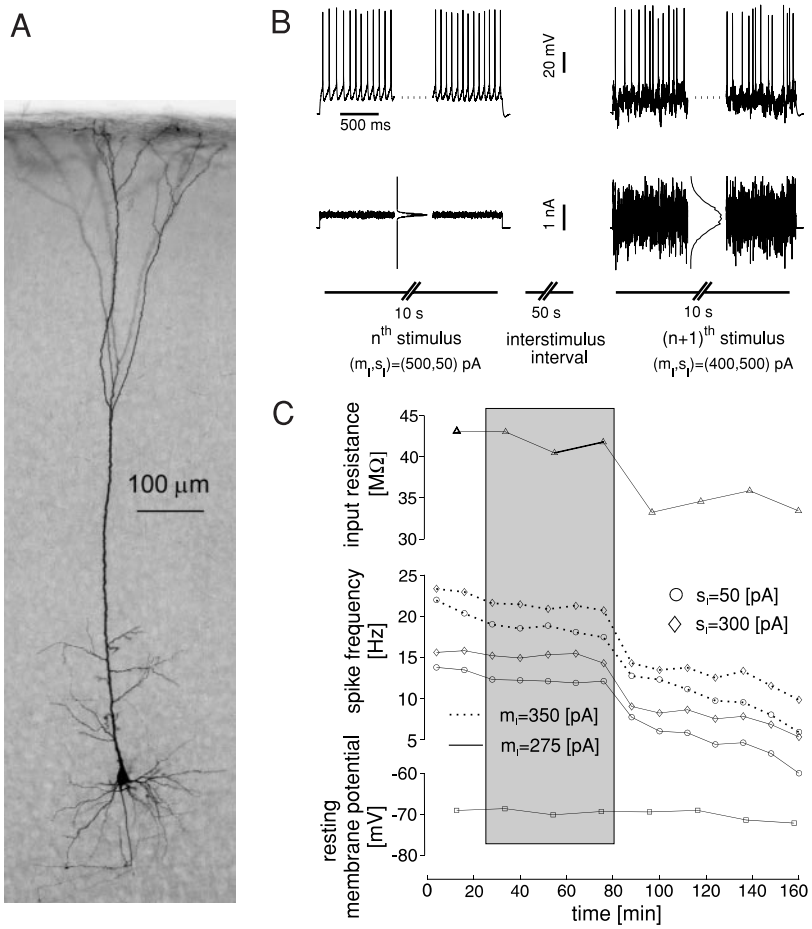

FIG. 1. Experimental procedure and stimulation protocol. *A*: typical layer 5 pyramidal cell of rat somatosensory cortex, filled with biocytin and stained according to ABC procedure (Hsu et al. 1981). Noisy currents were injected into soma in whole cell configuration. *B*: stimulation protocol is illustrated by showing two typical successive stimulations. Beginning and end of two stimulation currents are shown in *lower traces* and corresponding voltage recordings in *upper traces*. Cell started from resting potential (no stimulation) and was then driven by noisy current to state of sustained activity. In vivo–like current was generated as Ornstein–Uhlenbeck process (distributions of currents are shown in between interrupted *current traces*). Stimulation was 10 s long, or shorter if ≥150 spikes were collected (see METHODS). Each stimulation was followed by recovery time of ≥50 s. Early transient response (2 s) in which cell was adapting was not included in computation of spike frequency. Response function was calculated by measuring number of spikes in response to large number of different noisy currents. Two-dimensional space of parameters characterizing noisy current (m_I, s_I) was discretized and then points were explored in random order. *C*: response stability: input resistance, mean spike frequency, and resting potential as function of time. Data used for analysis were collected in period of 40–90 min (shaded region) during which mean spike frequency in response to same probe current was consistent (i.e., differences were comparable to error). This period was usually preceded by transient phase of several minutes of instability. Resting membrane potential was constant throughout whole session and hence is a bad indicator for checking response consistency of cell.

the same current was injected, the spike frequency did not change within the statistical error of *Eq. 5*), and by a final unstable phase. Cells with a stable period shorter than 40 min were not included in the analysis. Response consistency depended on the pipette solution. The cells were classified into three groups depending on the level of consistency: *1*) consistent cells: less than a third of the repeated recordings were out of range; *2*) poorly consistent cells: more than a third of the repeated recordings were out of range; and *3*) clearly inconsistent cells: errors as for poorly consistent cells plus there were clear inconsistencies at low frequencies (e.g., the frequency decreased with s_I for some points and increased for others). The number of consistent or poorly consistent cells was (out of total number): 41/44 for EGTA pipette solution, 14/19 for KGluc pipette solution, 6/12 for $KMeSO_4$ pipette solution.

Model of the integrate-and-fire neurons

The subthreshold dynamics of the only dynamic variable, the membrane voltage V, obey

$$C\frac{dV}{dt} = L(V) + I$$

where C is the membrane capacitance, $L(V)$ is the leakage, and I is the input current that is integrated until V is driven across the threshold θ and initiates an action potential. After the spike emission, V_r is reset to some value V_r from which the neuron starts again integrating the input current after a refractory period τ_r. For the leakage $L(V)$ we studied two models: *1*) the classical leaky integrate-and-fire neuron (LIF), which has a leakage proportional to the membrane depolarization $L(V) = -VC/\tau$ (τ is the membrane time constant); and *2*) the constant leakage integrate-and-fire neuron with a floor (CLIFF), which has a constant leakage $L(V) = -\lambda$. For this last neuron, to have the same behavior as for the LIF neuron, it is necessary to impose a rigid lower boundary for the depolarization, which we chose to be the cell resting potential (see *Response functions of the model neurons*).

Adaptation/facilitation components

The stationary response results from the combination of several dynamic processes occurring on different time scales. Some of them are likely to be transient and to disappear in a few hundreds of milliseconds (see RESULTS). Others are long-lasting and might reach a steady state on time scales of the order of seconds. When the effects of long-lasting processes merge together to produce a neuronal response with stationary statistics, we model them by introducing an additional current I_α proportional to the mean output spike frequency f. This current is meant to imitate any combination of adaptation and facilitation processes that determine the neuronal response in stationary condition. The linear dependency on f was suggested by the discrepancies observed between the best-fit theoretical response *without* adaptation/facilitation and the data. Moreover it is supported by the experiments that focus on specific components of frequency-dependent modifications of the input current. For example the calcium-dependent potassium current, which is responsible for fast adaptation, is usually modeled as a negative current proportional to the intracellular calcium concentration $[Ca^{2+}]_i$, which in turn is proportional to the spike frequency f. A possible implementation in terms of a detailed spike driven dynamics is as follows (see also Ermentrout 1998; Fuhrmann et al. 2002; Liu and Wang 2001 for related models): calcium (or whatever ion species is responsible for the phenomenon; see Powers et al. 1999; Sanchez-Vives et al. 2000) concentration is increased on every spike emission and then decays exponentially to its resting value

$$\tau_{Ca}\frac{d[Ca^{2+}]_i}{dt} = -[Ca^{2+}]_i + \alpha_{Ca}\sum_k \delta(t - t_k) \qquad (6)$$

where the sum extends over all the spikes emitted by the neuron up to time t (t_k is the emission time of the kth spike). If the dynamics of $[Ca^{2+}]_i$ are slow compared with the interspike intervals (i.e., $\tau_{Ca} \gg 1/f$), then $[Ca^{2+}]_i \simeq \alpha_{Ca} f$ and the current turns out to be proportional to the spike count in some temporal window, $I_\alpha = -\gamma\alpha_{Ca} f$. Any other model that, in stationary conditions, produces a negative current proportional to the mean spike rate would be equivalent.

Theoretical response functions

If the input current I is Gauss distributed and delta-correlated, then the equation for V can be written as

$$dV = \frac{L(V)}{C}dt + \mu dt + \sigma\sqrt{dt}\,\xi(t)$$

where ξ is a unitary Gauss-distributed variable that is updated every time step. For simplicity we focus on the CLIFF neuron, the same considerations apply to the LIF neuron. μ and σ^2 are the instantaneous mean and variance of the change in $V(t)$ per unit time and characterize the statistics of V on short time scales (see, e.g., Cox and Miller 1965). For a delta-correlated input current the variance of V grows linearly with time on short time scales and is proportional to σ^2. For such an input current, the response function can be computed analytically for both models (Fusi and Mattia 1999; Ricciardi 1977) and the expressions for the average firing rate $f = \Phi(m_I, s_I)$ is reported in Table 1. The CV of the interspike intervals can also be computed analytically. The expression can be found in Brunel (2000a) for the LIF neuron and in Fusi and Mattia (1999) and Salinas and Sejnowski (2002) for the CLIFF neuron.

The equations of Table 1 express the mean spike frequency f as a function of the mean μ and variance σ^2 in unit time of the input current (erf = error function). These parameters are related to m_I, s_I and the time correlation length τ_I as indicated in the bottom row: these expressions are based on the assumption that the input current has only fast synaptic components and hence the time correlation length τ_I is much shorter than the typical interspike interval. Indeed when the current of *Eq. 3* is injected, the variance of V is (Cox and Miller 1965)

$$\mathrm{Var}\,[V(\Delta t)] = \frac{\sigma_I^2\tau_I^3}{C^2}\left(\frac{\Delta t}{\tau_I} - 1 + e^{-\Delta t/\tau_I}\right)$$

TABLE 1. *Analytical expressions for the mean frequency f as a function of the statistics of the current (m_I, s_I) for the LIF neuron and the CLIFF neuron*

LIF Neuron	CLIFF Neuron
$f = \left\{\tau_r + \tau_m\sqrt{\pi}\int_{(V_r-\mu\tau_m)/\sigma\sqrt{\tau_m}}^{(\theta-\mu\tau_m)/\sigma\sqrt{\tau_m}} e^{x^2}[1+\mathrm{erf}\,(x)]\,dx\right\}^{-1}$	$f = \left[\tau_r + \frac{\theta - V_r}{\mu} + \frac{\sigma^2}{2\mu^2}(e^{-(2\mu\theta)/\sigma^2} - e^{-(2\mu V_r)/\sigma^2})\right]^{-1}$
$\mu = \frac{m_I}{C}, \quad \sigma = \frac{s_I\sqrt{2\tau_I}}{C}$	$\mu = \frac{m_I - \lambda}{C}, \quad \sigma = \frac{s_I\sqrt{2\tau_I}}{C}$

which in the limit $\Delta t \gg \tau_I$ scales as $(\sigma_I^2\ \tau_I^2/C^2)\ \Delta t = \sigma^2 \Delta t$, as expected from a delta-correlated process. For a more detailed analysis of the effects of time correlated currents on the response function see Brunel and Sergi (1998) and Fourcaud and Brunel (2002). These effects can be reabsorbed in an effective spike-emission threshold θ, which depends on σ_I.

The effects of adaptation/facilitation on the stationary response are introduced as an extra current ($m_I \rightarrow m_I - \alpha f$) proportional to the mean spike frequency. For each combination of m_I, s_I, the mean output frequency determines the amount of negative current that should be added to m_I and that modifies the output frequency. The process is iterated until the equation for the frequency becomes self-consistent and the frequency that appears in the negative current is the same as the output frequency

$$f = \Phi(m_I - \alpha f, s_I)$$

The asymptotic stationary response function and the response function with $\alpha = 0$ for the two model neurons are plotted in Fig. 5 and discussed in *Response functions of the model neurons*.

Data analysis and fitting procedure

The theoretical $f - m_I$ curves have been fitted to the stationary data. The fit was achieved through a Monte Carlo minimization (see e.g., Press et al. 1992) of the distance between the measured mean spike frequency f_k^{ex} and the theoretical spike frequency f_k^{th} predicted by the model

$$\chi^2 = \sum_k^N \frac{(f_k^{exp} - f_k^{th}(\mathbf{\Pi}))^2}{\Delta_k^2} \tag{7}$$

with respect to the set of parameters $\mathbf{\Pi} = \{\tau_r, Vr, C, \alpha\}$, plus τ_m or λ in case of the LIF or CLIFF neuron, respectively. Δ_k represents the confidence intervals defined in *Stimulation protocol and observables*. Because only 5 of the 6 parameters of the model neurons are independent, we set the threshold arbitrarily at $\theta = 20$ mV. In fact, both response functions (see Table 1) are invariant under the scaling $\theta \rightarrow \eta\theta$, $V_r \rightarrow \eta V_r$, $C \rightarrow C/\eta$, with $\eta > 0$.

The minimum χ^2_{min} of *Eq. 7* with respect to the parameters set $\mathbf{\Pi}$ follows approximately a χ^2-distribution with $N - M$ degrees of freedom, where N is the number of experimental points, and $M = 5$ is the number of free parameters. The fit was accepted whenever the probability $P(\chi^2_N - M \geq \chi^2_{min}$ was greater than 0.1 for consistent cells, and greater than 0.01 for poorly consistent cells.

In some cases we also report the *absolute discrepancy d*, defined as the average (across all points) absolute difference between the measured and the theoretical frequencies of the best-fit curves. This number is not correlated with the goodness-of-fit test and gives a useful indication of the error made in considering a theoretical response function which does not strictly pass the least-squares test.

RESULTS

Time development of the neuronal response

We measured the cell mean spike frequency in response to noisy currents with stationary statistics (see Fig. 1 and METHODS for details about the protocol). We identified at least three components of adaptation/facilitation, already known in the literature, which determine the features of the stationary response. What follows in this section is not meant to be an extensive and systematic analysis of all the factors that determine the stationary response. The goal is rather to clearly define what we mean by stationary response, to understand when it is possible to have it, and to summarize euristically all the observable mechanisms that affect the transient on different time scales and that might contribute to determine the stationary response. Such stationary response was usually reached in 1–2 s and then sustained until the end of the stimulation. For strong enough injected currents the cells were unable to sustain the elevated activity imposed by the stimulation and no stationary response was possible. The three components are illustrated in Fig. 2. Their features depend on the pipette solution and are summarized in Table 2. They are as follows.

- Initial adaptation (Schwindt et al. 1997): fast and invariably present for all the different preparations, it manifests itself for high enough spike frequencies: when the neuron is injected with a constant current, the second and successive interspike intervals are longer than the first one (see Fig. 2, *a3–a5*). This component, known in the literature to be attributed to calcium-dependent potassium current (see e.g., McCormick et al. 1985; Sah 1996), reaches a steady state in a few spikes and it is usually modeled as negative spike frequency–dependent current, which clearly affects the stationary response. This adaptation component was present for all the cells and all the preparations and in particular it was observed also in the strong presence of EGTA, a calcium chelator. Buffering of calcium concentration transients by EGTA is probably not fast enough to disrupt fast initial adaptation (Smith et al. 1984). The spike-frequency dependency was different depending on the pipette solution. The same effect was produced for lower currents in the case of EGTA pipette solution when compared with the case of KGluc pipette solution: 1.2 ± 0.4 nA (KGluc pipette solution), 0.6 ± 0.2 nA (EGTA pipette solution), corresponding to 36 ± 10 Hz (EGTA pipette solution) and 21 ± 8 Hz (KGluc pipette solution). For $KMeSO_4$ pipette solution: 0.8 ± 0.2 nA and 24 ± 7 Hz.
- Early facilitation: on a time scale of 1–2 s, the mean spike frequency slowly increases. This form of relatively slow facilitation was invariably present for the different preparations and shown by all of the recorded cells and for all the stimulation strengths (see Fig. 2). It is known in the literature to be attributed to calcium accumulation (Powers et al. 1999) and its effects on the stationary response compete with those of the late adaptation component (described below) when the spike frequency is high enough. For this reason it is difficult to isolate its effects and to characterize its dependency on the preparation. However, it was clear that early facilitation was mostly prominent when $KMeSO_4$ pipette solution was used and this would be compatible with the known fact (Zhang et al. 1994) that methylsulfate is the least disruptive to intracellular structures of calcium homeostasis.
- Late adaptation: for strong enough input currents the cells were unable to sustain the elevated activity imposed by the stimulation. After 2–3 s, the mean spike frequency estimated on a sliding temporal window was constantly decaying. The threshold current for detecting late adaptation and the rate of frequency decay depended on the preparation. In particular, the same effect (a frequency decay of more than 0.5 spikes/s) required relatively low currents in the case of EGTA pipette solution (0.8 ± 0.3

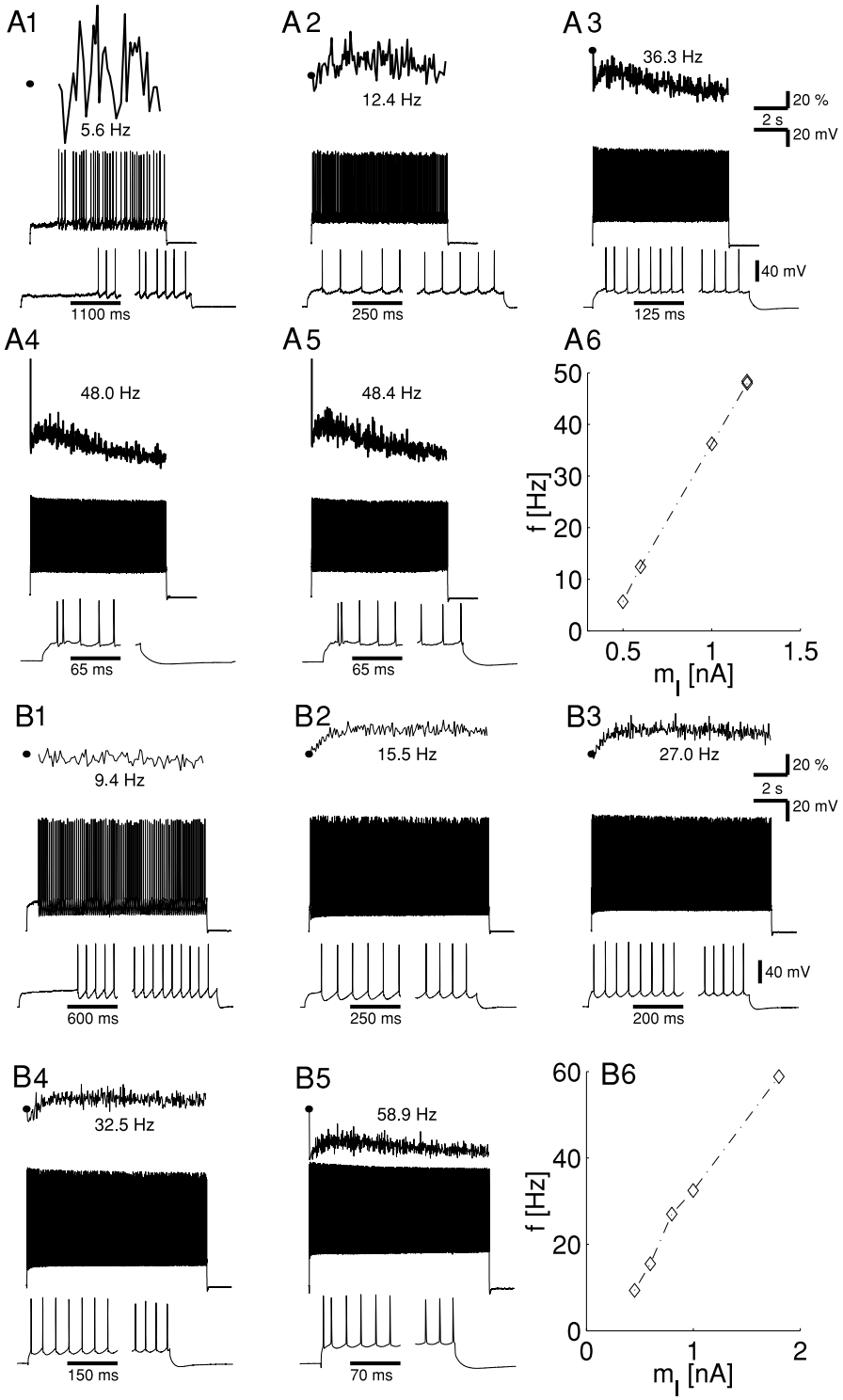

FIG. 2. Time course of neuronal response to different, increasing currents for two cells (with $s_I = 50$ and 0 pA, respectively). For each cell response to 5 input currents is shown in each of 5 panels in three ways: at *top* normalized instantaneous spike frequency (inverse of interspike interval times first interspike interval) as function of time (dots, when displayed, correspond to 100%); below it, *depolarization trace* and, at *bottom*, an enlargement of first and last portion of trace. *a6* and *b6*: mean spike frequency as function of input current m_I for 5 cases illustrated in the other 5 panels (*1–5*). As input current increases, both neurons show appearance of fast initial adaptation (first interspike interval is shorter than the second, starting from *a3* and *b4*), early facilitation, and slow adaptation (panels *3–5*). For small currents (*a1* and *b1*) both neurons show delayed response. Its link with early facilitation was not investigated. First neuron responds with doublets of spikes to strong enough currents (*a4–a5*). Early facilitation can cause steady output rate higher than that at beginning of spike train (*b2–b4*), and competes with slow adaptation at higher output rates (*a3–a5*, *b5*), where output rate at end of stimulation is smaller than that at beginning, causing response to be nonstationary in *a4–a5* (speed of decrease in spike rate of 1.66 Hz/s) and *b5* (1.17 Hz/s). Pipette solutions used were EGTA (cell *a*) and KGluc (see METHODS).

nA, corresponding on average to approximately 35 Hz for the 12 out of 13 cells that showed the phenomenon), higher for KGluc pipette solution (1.6 ± 0.5 nA, 52 Hz, all 19 cells), and much higher for $KMeSO_4$ pipette solution (1.8 nA and 60 Hz) for the few (3/12) cells that showed late adaptation. This kind of slow adaptation has already been studied (Fleidervish et al. 1996; Powers et al. 1999; Sanchez-Vives et al. 2000; Sawczuk et al. 1997; Schwindt et al. 1989) and it is hypothesized to be attributed to slow inactivation of sodium channels (Fleidervish et al. 1996; Powers et al. 1999; Sawczuk et al. 1997) and to an outward Na^+-dependent K^+ current (Sanchez-Vives et al. 2000; Schwindt et al. 1989). The spike frequency decay was always accompanied by a progressive drift of the maximal upstroke velocity of the membrane potential, indicating that the spike shape was continuously and slowly broadening. This phenomenon is best displayed by using longer stimuli that elicit high initial spike rates. An

TABLE 2. *Characteristics of the response over time: features of initial adaptation, late adaptation and maximal stationary response for EGTA pipette solution and for KGluc and $KMeSO_4$ pipette solutions for comparison*

Pipette Solution	Initial Adaptation		
	N	*I* (nA)	*f* (Hz)
EGTA	12/13	0.6 ± 0.2	21 ± 8
KGluc	19/19	1.2 ± 0.4	36 ± 10
$KMeSO_4$	12/12	0.8 ± 0.2	24 ± 7
	Late Adaptation		
	N	*I* (nA)	*f* (Hz)
EGTA	12/13	0.8 ± 0.3	35 ± 15
KGluc	19/19	1.6 ± 0.5	52 ± 11
$KMeSO_4$	3/12	1.8 ± 0.2	60 ± 5
	Max Stationary Frequency		
	N		*f* (Hz)
EGTA	11/13		44 ± 12
KGluc	5/19		56 ± 9
$KMeSO_4$	1/12		64

The onset currents and onset output frequencies are shown (values are average ± SD across different cells). *Early facilitation* (see text) is not reported in the Table because its characteristics were the same for all cells: the phenomenon was present for all output frequencies (i.e., the onset current was invariably the rheobase) with time constants of 1–2 s (see Fig. 2).

example is shown In Fig. 3*B*), where 60-s-long stimuli were used.

Many of the recorded cells (19/44) showed an initial doublet of spikes, resembling the beginning of a burst. This doublet sometimes masks the initial adaptation component and makes it difficult to analyze. Notice that all the recorded cells were selected not to be inherently bursting. The doublet was observed for all the preparations for strong enough stimulation (usually stronger than the one that reveals fast spike adaptation) and it is shown in Fig. 2, *a4–a5*. The threshold current depended on the pipette solution: 1.2 nA for the 4/13 in EGTA pipette solution, about 1.8 nA for 13/19 cells in KGluc pipette solution and for 2/12 cells in $KMeSO_4$ pipette solution. Because of its transitory nature, the mechanism responsible for this doublet probably does not affect the stationary response.

Maximal stationary response

The late adaptation component makes the cell unable to sustain a response with stationary statistics above a critical output spike frequency, which depended on the cell and on the pipette solution. Although the observed modifications in the spike mean frequency and in the spike shape were usually quite substantial at the end of long stimulations, all cells could recover during the interstimulus intervals, indicating that the phenomenon is reversible.

For most cells we did not stimulate for very long intervals ($\leq$60 s) as for the cell shown in Fig. 3. Hence we do not have enough data to determine the maximal stationary response for all cells. This analysis would have required the injection of several currents, strong enough to produce nonstationary responses, and it would have limited even further the number of stationary data points. Nonstationary responses are not included in the following analysis and are not modeled.

Usually we restricted the input currents to the range in which the slow frequency decay was below 1 Hz/s. This criterion restricted our analysis of the response function to a limited range of frequencies that depended on the pipette solution. The maximal frequency of this range could be determined for those cells for which the stimulation was strong enough to reveal a frequency decay above 1 Hz/s and it was (see Table 2): 44 ± 12 Hz (n = 11/13) for EGTA pipette solution and 56 ± 9 Hz (n = 5/19) for KGluc pipette solution. In $KMeSO_4$ pipette solution the cells did not display maximal stationary response with the exception of only one out of 12, in which case the maximal stationary frequency was 64 Hz.

Experimentally measured response functions

In Fig. 4 we show the response function as measured in the experiment. The measurements are shown in the form of $f - m_I$ curves that represent the output frequency f (the response) as a function of the mean current m_I at constant SD s_I. The CV of the interspike interval is also reported in the same form. The qualitative behavior was the same for all cells: for constant currents ($s_I = 0$), there is obviously no activity for average inputs that are below the rheobase current (i.e., the minimal constant current that makes the neuron fire), whereas the response curve is approximately linear for supra-rheobase currents. For noisy inputs ($s_I > 0$) there are essentially two regimes. *1*) A sub-rheobase, fluctuation-dominated regime in which the mean current m_I is below the rheobase current and hence not sufficient to drive the membrane voltage across the threshold for emitting a spike. In this case the action potentials are sporadically initiated by fluctuations and hence the spike activity is very irregular and the CV is high (Fig. 4*C*). *2*) A supra-rheobase, drift-dominated regime, in which the membrane potential fluctuates around a rising ramp that leads to the emission threshold at a more regular pace (Fig. 4*B*). The introduction of noise permits sub-rheobase activity, which in turn smooths out the response curves at the rheobase. The curves, convex for weak input currents, sometimes bend at high frequencies (see e.g., Fig. 6, *B* and *C*) and hence change curvature.

Response functions of the model neurons

The data points have been fitted by the response functions of two simple model neurons sharing a similar qualitative behavior (see METHODS). The two models differ in the form of the leakage $L(V)$: for the first, classical leaky integrate-and-fire (LIF) neuron the leakage is proportional to V [$L(V) = -VC/\tau_m$, where τ_m is the membrane time constant], whereas for the second model—the CLIFF neuron—the leakage is constant [$L(V) = -\lambda$] and the input current is integrated linearly. To obtain two qualitatively similar response functions for the two models, it is essential to limit the membrane potential from below in the case of the CLIFF neuron (Fusi and Mattia 1999; Salinas and Sejnowski 2002). Indeed, when both neurons are injected with a sub-rheobase noisy current, the variance of the fluctuations of the membrane voltage tends to increase linearly with time. However, for the LIF neuron the leakage compen-

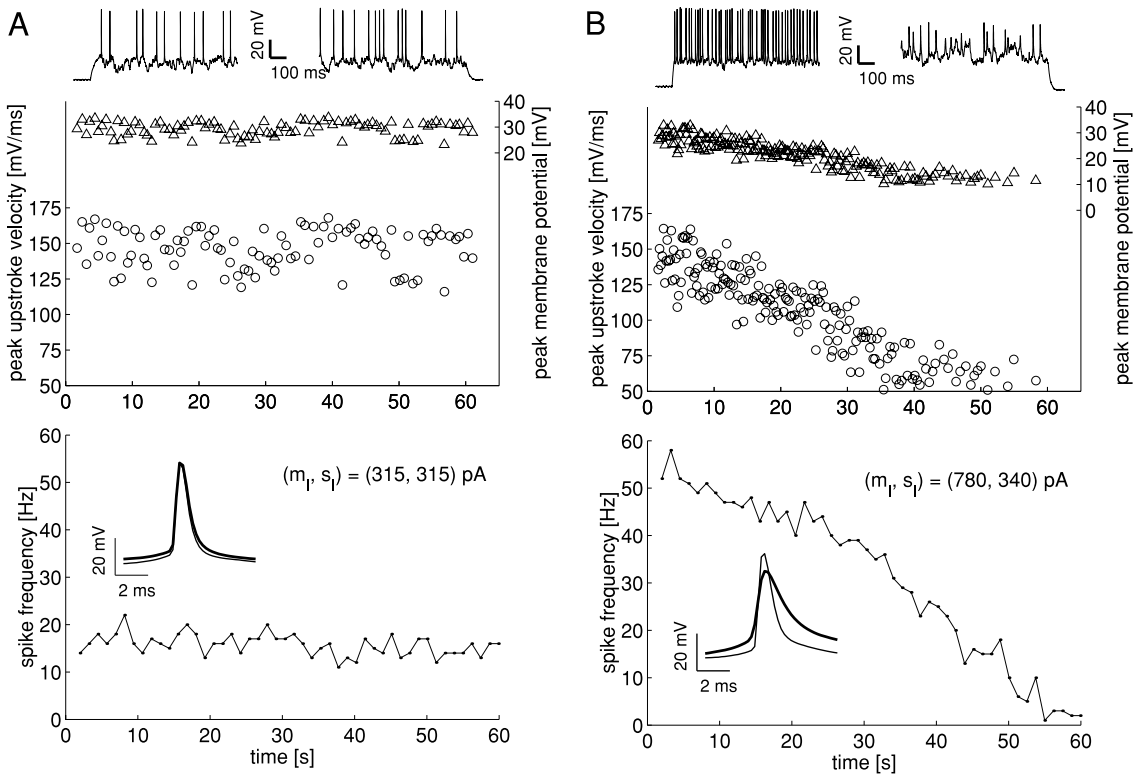

FIG. 3. Response stationarity: example of stationary (*A*) and nonstationary (*b*) response of same cell to two different stimuli. Stimulation was unusually long (60 s) to better expose difference in responses. *a* and *b*, *top to bottom*: voltage traces at beginning and end of stimulation, peak membrane potential (triangles), peak upstroke velocity (circles), shape of action potential at beginning (thin line) and at end (thick line) of stimulation (average across 20 spikes), and spike frequency estimated on a 1-s sliding time window as function of time. *a*: response is stationary and statistics of all observed quantities did not change throughout long stimulation interval. When same cell was injected with strong current (*B*), it showed a nonstationary response: elevated rate to which neuron would have been driven by stimulation could not be sustained. Both peak upstroke velocity and peak membrane voltage decayed in time, indicating that continuous decrease in mean spike frequency is accompanied by broadening of spike shape. Action potential almost completely disappeared over time and could hardly be distinguished from large voltage fluctuations induced by current. Voltage deflection was considered as a spike if peak upstroke velocity was greater than threshold value (50 mV/ms). Ultimately some fluctuations are not detected as spikes, and cell stopped firing according to our criterion, but completely recovered in interstimulus interval.

sates for this tendency, and, depending on the parameters of the current, can lead to a stationary sub-rheobase regime in which *V* fluctuates around an asymptotic value. For the CLIFF neuron this is not possible because the current is integrated linearly and all the fluctuations accumulate: for negative net currents (mean synaptic current minus leakage) the mean voltage de-

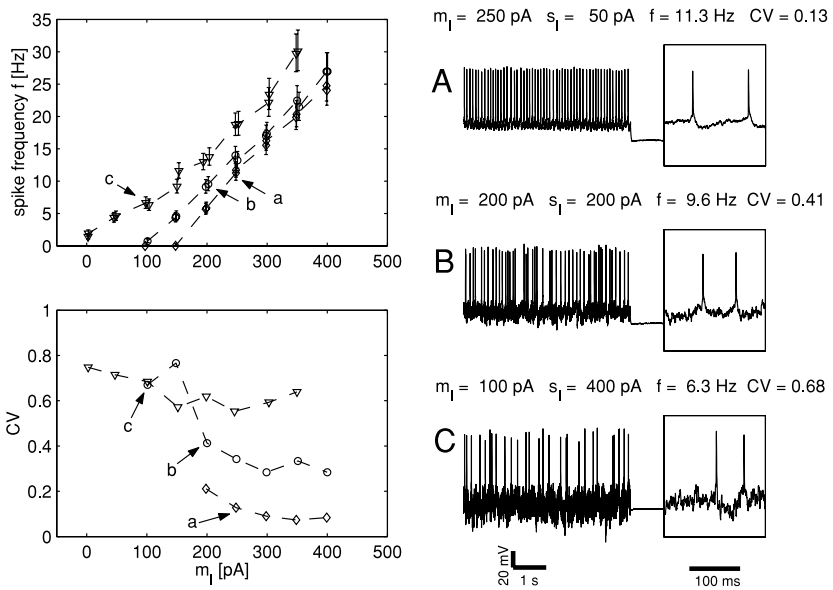

FIG. 4. Experimentally measured response functions. Example of response function as measured in experiment, shown by f–m_I (*left plot*) *curves* that represent output frequency f (response) as function of mean current m_I at constant SD s_I. Data points represent mean spike frequency in stationary conditions (error bars estimated as in *Eq. 5*). Corresponding coefficients of variability (CV) of interspike intervals, measuring degree of irregularity of spike trains, are plotted below. Membrane voltage traces for three points are shown in *right panel*, together with enlargement (*right insets*). Note that many frequencies have been measured twice, at different times: responses to same current were consistent, indicating that recordings were stable. Qualitative behavior is same for all cells: for almost constant inputs (*bottom curve*, $s_I = 50$ pA), there is no activity for sub-rheobase currents (i.e., $m_I < 150$ pA), whereas *response curve* is approximately linear for supra-rheobase currents. Spike train is regular (*A*). For noisy currents (*top curves*, $s_I = 200$ and 400 pA) there are two regimes: *1*) supra-rheobase, drift-dominated regime similar to case of constant current (*b*) and *2*) sub-rheobase, fluctuation-dominated regime in which spike activity is irregular (*c*).

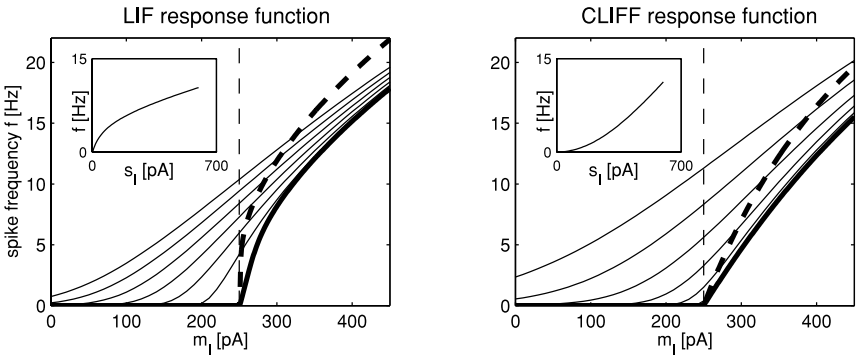

FIG. 5. Comparison between response functions of LIF neuron (*left*) and of CLIFF neuron (*right*). *Curves in plots: output mean spike frequency* f *as function of mean current* m_I at constant s_I (as in Fig. 4). *Insets*: *f* is shown as function of s_I for constant m_I (at rheobase m_I = 250 pA). Thick lines: response function to constant currents with (solid) or without (dashed) frequency-dependent modification of input current. Seven *f–*m_I *curves* correspond (from *bottom* to *top*) to s_I = 0–600 pA, at steps of 100 pA. Response functions are similar to measured curves of Fig. 4. Thus same considerations apply to theoretical response functions. Main qualitative difference between responses of the two model neurons is exposed in *insets* and resides in dependency on s_I (see text). Note how frequency-dependent term linearizes response at rheobase current (vertical dashed line) (Ermentrout 1998).

creases and the fluctuations increase boundlessly. In such a sub-rheobase regime the average spike frequency of the CLIFF neuron is always zero (Fusi and Mattia 1999; Gerstein and Mandelbrot 1964). The rigid barrier that limits the membrane voltage from below permits the neuron to fluctuate steadily around a value near the lower barrier, waiting for a fluctuation

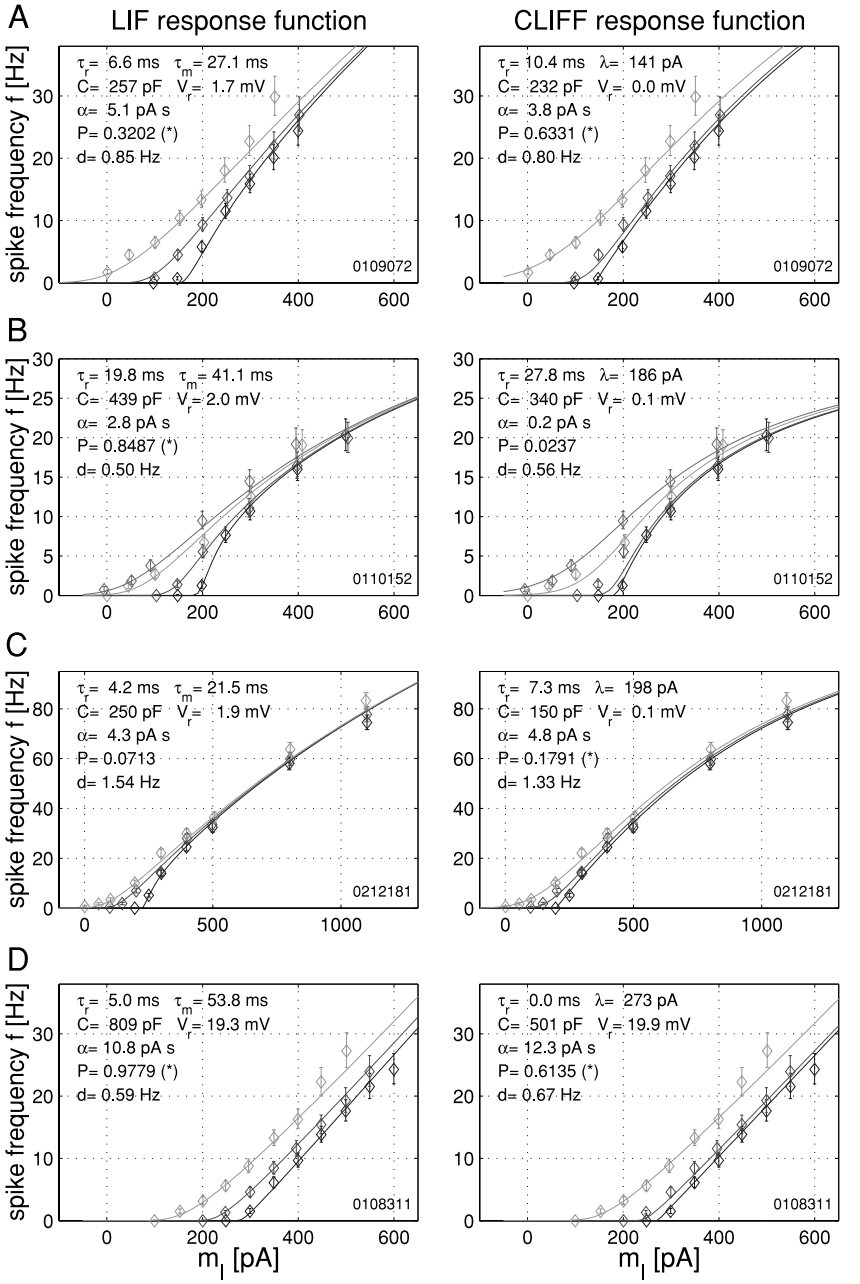

FIG. 6. Fitting theoretical response functions to experimental data. LIF (*left*) and CLIFF (*right*) response functions (full lines) fitted to experimental mean frequencies (diamonds) from 4 cells are shown (error bars as in *Eq. 5*). Each row corresponds to a different cell. Response functions are shown as $f - m_I$ curves at constant s_I (s_I = 50, 200, 400 for *A* and *D*, s_I = 50, 200, 400, 500 for *B*, s_I = 0, 200, 300 pA for *C*) as in Fig. 4. *Top left part of each plot*: effective parameters resulting from fit. *P* expresses goodness-of-fit (see METHODS for exact definition): high values indicate a good match between data and theoretical response functions. For cells shown values above 0.1 indicate that fit passed χ^2 test. *D* is *absolute discrepancy*, defined as average (across all points) absolute difference between measured and theoretical frequencies. This number is not correlated with goodness-of-fit test, being below 2 Hz even when fit was to be rejected. *A*: cell that can be fitted by both models; *B*: cell that can be fitted by LIF response function only; *C*: cell that can be fitted by CLIFF response function only; *D*: cell that can be fitted with limit parameter values only (see text): sensitivity to s_I is high and the $f - m_I$ curves do not tend to converge to common asymptotic value for large m_I. (All cells in EGTA pipette solution.)

that drives V across the threshold. In this case a sub-rheobase regime with nonzero frequency is possible.

In both neurons the adaptation/facilitation components which determine the asymptotic stationary response were modeled by assuming that the effective mean current driving the cell is reduced by a term proportional to the cell's own spike frequency ($m_I \rightarrow m_I - \alpha f$; see METHODS). There are several simple and detailed biophysical models that correspond to this phenomenological model: the simple models based on calcium dependent potassium channels (see e.g., Wang 1998) and the more realistic Hodgkin–Huxley type model in Traub and Miles (1991) are but two examples (see also Ermentrout 1998). All these models exploit the fact that the adaptation/facilitation processes are slow compared with the average interspike intervals. Note that these mechanisms do not account for the nonstationarity observed in Fig. 3*B*, given that our model neuron can always have a stationary response, no matter what the intensity of stimulation.

The response functions corresponding to the two models are plotted in Fig. 5 in the same way as the measured curves are shown in Fig. 4. The main difference between the two model neurons is in the dependency of the spike frequency on s_I, the fluctuations amplitude of the noisy current: the CLIFF neuron is more sensitive to large s_I and this fact manifests itself in a progressively increasing distance between the $f - m_I$ curves. This behavior can be exposed by plotting the spike frequency as a function of s_I at constant m_I (*insets* in Fig. 5): the curvature has a different sign for the two neurons. Moreover the response function of the LIF neuron without adaptation/facilitation components is highly nonlinear around the rheobase current for low levels of noise and, for $s_I = 0$, the derivative of the $f - m_I$ curve is infinite. These nonlinearities are attenuated by the frequency-dependent feedback (Ermentrout 1998).

The CV of the interspike intervals behave in the same way for the two model neurons: in the sub-rheobase fluctuations dominated regime the CV is close to 1 for a wide range of input currents. This corresponds to the maximal irregularity and the train of spikes has Poisson statistics. As the current drives the neuron toward a drift-dominated regime, the CV approaches 0 with a speed that depends on s_I (i.e., the fluctuations in the input current).

Fitting the theoretical response functions to the data

Both models could faithfully reproduce most of the cells stationary responses, at least for those neurons that had consistent enough responses to allow for a quantitative analysis (see METHODS). For each cell we fitted the theoretical response functions to the data points by searching the space of the 5 independent parameters characterizing each model: the capacitance C, the refractory periodτ_r, the reset potential V_r, the adaptation/facilitation constant α, and the time membrane constant τ_m for the LIF neuron and C, τ_r, V_r, α, and the leakage λ for the CLIFF neuron (see METHODS). We adopted a Monte Carlo technique that minimizes the mean square distance between the data points and the predicted values, each point being weighted by the inverse of the confidence interval. The χ^2 test passed either with one model or with the other (or with both) with a probability $P > 0.1$ for 27 consistent cells out of 37. For all these cells, the EGTA pipette solution was used. For other pipette solutions the consistency was usually poor and the χ^2 test passed with a probability $P > 0.01$ for 16 cells out of 24.[1] The responses could anyway be well approximated by the theoretical functions even when the models did not pass the test: the average discrepancy between the measured and the model frequencies were <2.5 Hz; <1.5 Hz if frequencies below 50 Hz were considered. That is, the average difference between a single data point and its theoretical match was below 3 Hz even when the test did not pass. Examples of fitted response functions are shown in Fig. 6. The LIF model was best suited to reproduce $f - m_I$ curves that were almost equally spaced (Fig. 6*B*), whereas the CLIFF model could capture better those cells that were less sensitive to low levels of noise as in Fig. 6*A*.

Adaptation/facilitation components of the model dynamics turned out to be essential to fit the response of the models to the data. For the LIF neuron it is necessary to linearize the response function at the rheobase. For the CLIFF neuron, which already has an almost linear $f - m_I$ curve at the rheobase, one might wonder if the fitting would have been possible without adaptation/facilitation components. Increasing the membrane capacity C as well as increasing α reduces the slope of the $f - m_I$ curves. However, in contrast to adaptation/facilitation, an increased capacity also reduces the effect of fluctuations on the spike frequency and hence diminishes the sensitivity to s_I. Thus for the CLIFF neuron, adaptation/facilitation are the only mechanisms that can change the slope of the $f - m_I$ curves almost without affecting the distance between $f - m_I$ curves that correspond to different values of s_I (La Camera et al. 2002).

For high frequencies (>40–50 Hz) there is a preliminary evidence of a phenomenon that is not captured by our model neurons: the $f - m_I$ curves corresponding to different s_I have a slight tendency to diverge, as if the sensitivity to s_I would increase for strong enough stimulation (see, e.g., Fig. 6*C*). This is not captured by our models of integrate-and-fire neurons for which asymptotically the $f - m_I$ curves always tend to merge. This divergence effect is a source of discrepancy that usually does not compromise the χ^2 test, but that clearly indicates the activation of an extra process that is not modeled. The increased sensitivity to s_I is usually accompanied by an increase in the CV of the interspike intervals (see the previous section) and it might be attributable to the activation of calcium spikes in the distal dendrite (Larkum et al. 1999). The study of this phenomenon will require further investigation.

Some cells ($n = 6$, all of them in EGTA pipette solution) could be fitted only by searching a region of limit parameter values, letting the reset potential be very close to the threshold. This was the only way to capture sets of $f - m_I$ curves that do not tend to converge to a common asymptotic value for elevated currents (Fig. 6*D*). Although the response function could be described by the theoretical response function, we do not consider the model as appropriate for describing these cells. The theoretical response functions are computed under the assumption that the current is delta-correlated, and this is not a good approximation when the reset potential is very close to the threshold. Hence we consider these cells belong to a

[1] For poorly consistent cells the purely statistical error underestimates the error, and a lower threshold for P was chosen. This threshold corresponds in average to multiplying the statistical error by a factor up to 1.25 at most.

different class that the simple integrate-and-fire models are probably inappropriate to describe.

We recorded the response of 10 cells to noisy currents with a longer time correlation length ($\tau_I = 5$ ms). The $f - m_I$ curves were qualitatively the same as in the case of shorter τ_I and they could be fitted by the theoretical response functions of Table 1 (not shown), even if they are valid only for delta-correlated currents. A full account of the analysis of these cells will be reported elsewhere.

Higher-order statistics of the interspike intervals

The main goal of this investigation was to study the neuronal response in terms of mean spike rates. However, it is also interesting to consider the higher-order statistics of the distribution of the interspike intervals. A detailed and systematic analysis would require more data to estimate the higher-order moments of the distribution, although our preliminary analysis of the variance of the interspike intervals already gives interesting indications. In Fig. 7 we plotted, for two cells, the CV of the interspike intervals as a function of the spike frequency. Each curve is obtained by keeping s_I fixed and then sweeping along m_I. The parameters of the model are tuned to fit *only* the mean firing frequencies. Then, with the best-fit parameters we computed the CV by means of simulations and compared it to the measured one.

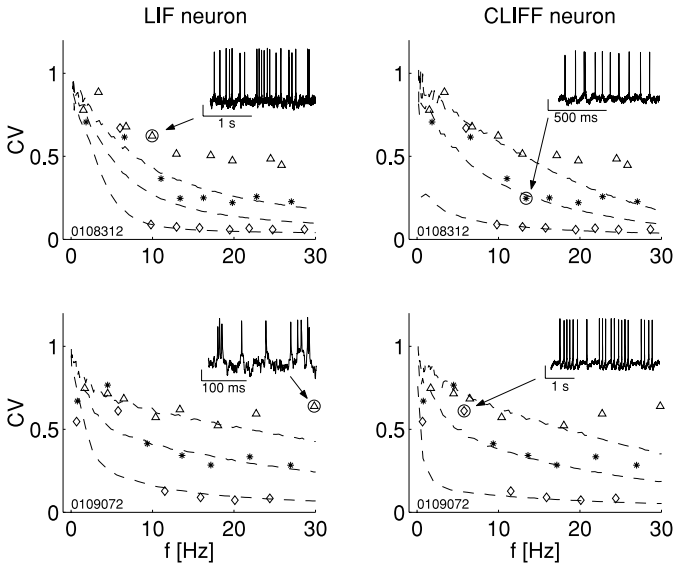

FIG. 7. Higher-order statistics of interspike intervals: predicting coefficient of variability (CV) for interspike intervals. Parameters of cells were determined by fitting mean firing rates and then used to predict CV for same statistics of current. Two rows correspond to two different cells: *top*, a typical cell; *bottom*, our best-fit cell. CV is plotted against mean spike frequency and data points (different symbols, depending on s_I) are compared with CV predicted by LIF model (*left*) and to CLIFF model (*right*). Each curve in plot is obtained by setting s_I to a fixed value and then sweeping along m_I. Values of s_I: 50, 200, and 400 pA. Only points corresponding to finite spike frequency (i.e., larger than 0.2 Hz) were considered to avoid huge fluctuations of CVs, which would make figure hardly readable. Although parameters were tuned to capture mean frequency only, predicted CV is in good agreement with measured one for a wide range of frequencies. *Insets*: typical *voltage traces* corresponding to 4 different statistics of input currents (corresponding CV points are circled): *top left*: typical irregular response to noisy current; *top right*: regular spike train in response to current with low s_I; *bottom left*: doublets and bursts of spikes for high and s_I and m_I; *bottom right*: response to a current near rheobase for low s_I.

The cell in the *top row* of Fig. 7 represents the typical case, whereas the one below is our best fit. The agreement between the predictions and the data points is in general reasonably good for most of the points and for most of the cells, even if it would probably not pass a χ^2 test. The largest discrepancies are observed at high firing frequencies, for elevated values of the variance of the input current. There are at least two reasons for these discrepancies. First, these points might not be completely stationary, given that the firing frequency approaches the maximal allowed value for the cell. As expected, this produces a higher CV than predicted by the theoretical models for which the nonstationarity is not modeled. Second, at high frequencies and high s_I we often observed doublets or bursts of spikes (see the *bottom left inset* in Fig. 7). This is also not captured by the model and increases the measured CV.

Moreover there is often a large discrepancy around the rheobase current, when the amount of noise in the current is small. Near the threshold for spike emission, the response sometimes consisted of sequences of tonic, regular firing interrupted by periods of subthreshold activity (see the *bottom right inset* in Fig. 7). This behavior, not captured by a simple integrate-and-fire model, artificially increases the variability of a train of spikes that otherwise would be rather regular.

Effective parameters

The parameters corresponding to the best fit must be considered as *effective* parameters, that is, as those parameters that provide the best description of the stationary response function. Other observables might not be captured by the same parameters (also see DISCUSSION). Fitting the $f - m_I$ curves for three different values of s_I was already restricting the model parameters to a small region of the parameter space (we had 3 to 5 $f - m_I$ curves for each cell). The range in which single parameters can vary and the χ^2 test still passes depends on the sensitivity of the spike frequency on the different parameters. A rough estimate indicates that the least determined parameters are τ_r (up to about $\pm 70\%$ error) and V_r (about $\pm 25\%$ error), whereas the other parameters can vary at most in intervals of the order of $\pm 20\%$ (α, CLIFF neuron), $\pm 5\%$ (C, α, τ, LIF neuron; C, λ, CLIFF neuron). The refractory period is clearly the effective parameter to which the response function is least sensitive because it affects mostly the very high-frequency region ($f \sim 1/\tau_r$), usually beyond the observed range of output rates.

The effective parameters for the two model neurons are reported in Table 3 for all the cells that were consistent or poorly consistent and that did pass the χ^2 test (the number of cells is reported in column N). For the analysis of effective parameters we mainly focused on the cells with EGTA pipette solution because they were stable enough to give consistent responses for a large number of data points. The parameters are reported as an average across all cells with EGTA pipette solution and separately for the other two pipette solutions. Interestingly, the differences between different pipette solutions were usually comparable to the differences across cells (reported as SD).

Two passive parameters characterizing the cell (τ_m, C) could be measured directly (see METHODS), and their values were in general different from the *effective* parameters. The cross-correlations were negligible for the CLIFF neuron and weak

TABLE 3. *Average parameters that best fit the model response functions to the data (effective parameters), together with the passive parameters measured directly in the experiment (bottom)*

Pipette Solution	LIF Neuron					
	N	τ_r (ms)	C (nF)	V_r (mV)	α (pA · s)	τ_m (ms)
EGTA	17/41	9.3 ± 7.1	0.57 ± 0.35	0.2 ± 12.2	3.5 ± 2.6	35.4 ± 13.3
KGluc	4/14	9.4 ± 6.5	0.53 ± 0.29	9.9 ± 10.2	10.8 ± 6.3	26.3 ± 13.2
$KMeSO_4$	3/6	1.0 ± 1.5	0.75 ± 0.30	−10.1 ± 20.0	4.8 ± 4.2	38.4 ± 3.0
	CLIFF Neuron					
	N	τ_r (ms)	C (nF)	V_r (mV)	α (pA · s)	λ (nA)
EGTA	25/41	16.3 ± 8.9	0.28 ± 0.07	0.1 ± 0.1	3.6 ± 2.0	0.30 ± 0.12
KGluc	6/14	16.6 ± 6.7	0.22 ± 0.04	0.2 ± 0.6	4.5 ± 3.5	0.41 ± 0.07
$KMeSO_4$	3/6	9.8 ± 12.5	0.15 ± 0.13	0.0 ± 0.0	7.1 ± 2.2	0.27 ± 0.13
	Directly Estimated Parameters (LIF-Fitted Cells)					
	N	R (MΩ)	C (nF)	—	τ_m (ms)	Age
EGTA	17/41	41 ± 14	0.46 ± 0.32	—	16.4 ± 5.8	20.8 ± 7.9
KGluc	4/14	27 ± 5	0.89 ± 0.15	—	23.8 ± 2.5	27.0 ± 2.7
$KMeSO_4$	3/6	23 ± 1	1.03 ± 0.21	—	23.7 ± 5.3	25.7 ± 3.2
	Directly Estimated Parameters (CLIFF-Fitted Cells)					
	N	R (MΩ)	C (nF)	—	τ_m (ms)	Age
EGTA	25/41	38 ± 13	0.51 ± 0.30	—	17.1 ± 6.2	22.4 ± 9.0
KGluc	6/14	24 ± 3	1.00 ± 0.05	—	23.8 ± 2.9	27.0 ± 2.1
$KMeSO_4$	3/6	35 ± 20	0.81 ± 0.28	—	24.9 ± 3.3	23.0 ± 3.5
	Directly Estimated Parameters (All Cells)					
	N	R (MΩ)	C (nF)	—	τ_m (ms)	Age
EGTA	41	40 ± 12	0.45 ± 0.26	—	16.1 ± 5.5	21.9 ± 8.6
KGluc	19	24 ± 7	0.99 ± 0.20	—	23.1 ± 2.6	27.0 ± 2.3
$KMeSO_4$	12	28 ± 13	0.92 ± 0.29	—	23.2 ± 3.3	24.8 ± 3.1

Values are average ± SD. The parameters are reported for the EGTA pipette solution (mostly consistent responses) and, for comparison, for the other two pipette solutions for which the statistics is poorer (the cells responses were less consistent). N is the fraction of cells used for determining the average parameters (i.e., the cells which passed the χ^2 test with $P > 0.1$ for consistent cells, and $P > 0.01$ for poorly consistent cells. See Fig. 6 for a few examples). The parameters of the two models are defined in the text. Note that the threshold θ is set to 20 mV and the resting potential is 0 mV for both neurons (see METHODS).

for the LIF neuron: the correlation between the directly measured capacitance and the effective capacitance of the LIF neuron was 0.59 (0.03 for the CLIFF neuron), and the correlation between the membrane time constants was 0.30. Because real neurons are not integrate-and-fire neurons, such a mismatch is not very surprising. Indeed, the effective parameters provide a good fit to the mean spike frequencies, while the passive membrane parameters are estimated from very different observables (the subthreshold response to short pulses), in different experimental conditions. No clear patterns between effective or directly measured parameters and the model that could fit the data emerged.

DISCUSSION

The most prominent result of the present work is that simple integrate-and-fire model neurons can faithfully recreate the response of neocortical pyramidal cells to in vivo–like currents. We also gave a full account of the dependency of the cell response on the fluctuations of the input current (s_I), which has usually been overlooked in previous studies of neural response properties. This dependency was recently shown to play an important role when the neuron works in a sub-rheobase regime (Amit and Brunel 1997; Amit and Tsodyks 1991; Chance et al. 2002; Fusi and Mattia 1999) or when a network of interacting neurons has to respond fast to a time varying input (Rudolph and Destexhe 2001; Silberberg, Bethge, Markram, Tsodyks, and Pawelzik, unpublished observations, 2002).

The agreement between the theoretical and the measured response function is remarkably good for a wide range of statistics of the input currents, on the whole $\{m_I, s_I\}$ space and for all the sustainable spike frequencies of the analyzed cells. Hence, our results cover a variety of physiological scenarios that can be studied by measuring the neural response when moving along specific trajectories in the $\{m_I, s_I\}$ space. For instance balanced synaptic input, as studied e.g., in Chance et al. 2002, would correspond to increasing the variability of the current s_I, while keeping the mean current m_I fixed, and the outcome could be predicted by studying the theoretical response function of integrate-and-fire neurons.

Moreover the knowledge of the response functions to in vivo–like currents allows one to study many dynamic properties of networks of interacting neurons and to relate single neuron properties to the activity observed in in vivo experi-

ments. For instance, imposing the stability of a network state, like spontaneous activity (Amit and Brunel 1997), can constrain the possible architecture of the network, thus providing an indirect measurement of the synaptic efficacies in vivo. This will require a more extensive analysis of different types of cells, in different layers and different areas. The analysis of the dynamic states of a network of neurons will also require an additional study of the dependency of the parameters m_I, s_I of the current on the mean output rate of the presynaptic neurons. This dependency can be quite complicated, involving for instance the short-term dynamics of single synaptic responses (Tsodyks et al. 1998), the effects of a particular morphological structure (Rhodes 1999), or calcium dynamics (Larkum et al. 1999). So far the analysis of the in vivo phenomena based on single neuron response functions has been successfully performed with a simple linear relation between both m_I and s_I^2 and the spike frequency of the presynaptic neurons (Amit and Brunel 1997; Brunel and Wang 2001; Fusi and Mattia 1999; Yakovlev et al. 1998).

Besides these additional studies, many novel issues are raised by this work and remain open for further investigation. Here we focused on a specific observable, the mean spike frequency, to conclude that pyramidal cells respond very much like integrate-and-fire neurons. This is just a starting point and there are other aspects and observables of the neural activity to be investigated. The analysis of the CV that we present here provides a preliminary indication that integrate-and-fire neurons can capture more than the mean spike frequency. Because the fluctuations play an important role in determining the exact times of the initiation of the action potential (Mainen and Sejnowski 1995), it would be interesting to see how well the integrate-and-fire neuron (or related models) can describe the exact spike times under noisy current injection (see Kistler et al. 1997). This issue was beyond the scope of this report, but is currently under investigation (R. Jolivet, A. Rauch, H. R. Lüscher, and W. Gerstner, unpublished observations; M. Larkum, W. Senn, and H. R. Lüscher, unpublished observations).

A more systematic analysis of higher-order statistics of the spike trains and to what extent the exact timing of the spikes can be reproduced by the same simple integrate-and-fire neurons will be studied elsewhere and will probably require the introductions of new elements in the neuron model. Besides, such a study will certainly further constrain the effective parameters (e.g., the reset potential V_r can be determined more precisely by fitting both the mean frequency and the CV). So far, both the LIF and CLIFF neuron models with adaptation/facilitation are good enough to describe the response function of pyramidal cells, at least for the wide, biologically plausible range of input currents that was investigated in our work. Other observables might better expose the differences between the two models.

The response of the cell under strong persistent stimulation has not been modeled here. When neurons cannot sustain the elevated rate to which they would be driven by the input current, it is not possible to define a stationary response function. This behavior has to be incorporated in the model that, so far, can reliably describe the response function of the neuron only when sustained spike frequencies are below the threshold frequencies indicated at the end of *Maximal stationary response* (30–80 Hz depending on the pipette solution used). Above these frequencies some other mechanism beside fast or slow spike frequency adaptation should be invoked to capture the effective reduction of the spike frequency. The activation of such a mechanism cannot rely only on the number of emitted spikes because this would not account for the behavior illustrated in Fig. 3*b*, where the cell eventually stops firing. Therefore it is more likely to depend on some dynamic variable related to the average depolarization of the cell. One possibility is the inactivation of sodium channels, which has already been identified as responsible for late adaptation in other works (Fleidervish et al. 1996; Powers et al. 1999; Sawczuk et al. 1997).

An important element of realism that was not considered so far concerns the way synaptic conductances are imitated by the injection of a current into the soma. Generating real synaptic inputs by activating presynaptic neurons is the most realistic (and challenging) way of providing in vivo–like inputs to the neurons. However, it is interesting to study intermediate steps toward a realistic situation. Many investigators (see, e.g., Destexhe et al. 2001 and references therein) imitate synaptic conductances by generating a somatic current that is a product of a Gauss-distributed conductance multiplied by a voltage-dependent driving force (the instantaneous membrane voltage minus the reversal potential). We give in the APPENDIX a detailed description of this procedure. This kind of time varying current can be generated in an experiment by using dynamic clamp techniques (see, e.g., Harsch and Robinson 2000). The distribution of the injected current is not distorted much by the voltage-dependent driving force, and thus the final total current can still be reasonably approximated by an Ornstein–Uhlenbeck process (see also Amit and Tsodyks 1992). However, to study the effective response function of the neuron, the correct scaling factors for both the mean and the variance of the current should be introduced. These factors depend on the average membrane voltage, which in turn depends on the parameters of the current. As a consequence, the scaling factors in principle might not be the same for all points of the $f - m_I$ curves whose shape might be qualitatively different when conductances are considered (Tiesinga et al. 2000). Moreover, conductance-based inputs shorten the effective time correlation length of the membrane depolarization (see, e.g., Paré et al. 1998), which in turn modifies the effective threshold for emitting a spike (Brunel and Sergi 1998). However, the analysis presented in the APPENDIX shows that even when a *unique* scaling factor for all the input currents is chosen, the distortions of the stationary response functions are negligible and the neuron responds in a similar way to either current injection or conductance drive. There is a preliminary evidence that also transient responses are not substantially modified when the voltage-dependent driving force is considered: the differences are quantitative and not qualitative (Fourcaud and Brunel 2002). As a consequence, the effects of the voltage-dependent driving force can be compensated by the introduction of some *constant* factors that multiply the total excitatory and inhibitory currents. These factors might change dramatically the relation between the frequencies of the presynaptic neurons and the statistics of the input current, but they do not affect the results presented in this work, which are more related to the dependency of the output spike frequency on the statistics of the input current.

APPENDIX

Conductance versus current injection

The response function studied in our experiments allows relating the output spike frequency to the statistics of the input current—here described by the pair $\{m_I, s_I\}$—that in turn depends on the mean frequency of the input synaptic events and on their efficacy (see *Eqs. 1* and *2*). In particular, if the inputs can be grouped into two classes (excitatory and inhibitory), then the pair depends on a quadruplet of parameters: $\{N_e f_e, \bar{I}_e, N_i f_i, \bar{I}_i\}$ (see METHODS for the definition of the symbols). Given the response function $f = \Phi(m_I, s_I)$ and the relation between $\{m_I, s_I\}$ and the quadruplet mentioned above, one can study the dynamic properties of an arbitrary number of homogeneous populations of neurons. For instance the stability of a single recurrent network of excitatory cells can be analyzed by imposing that the input spike frequency f matches the output spike rate f of any of the cell: $f = \Phi([m_I(f), s_I(f)]$. In general, what really matters is the relation between the output spike frequency and the input spike frequency of all the presynaptic populations of neurons.

To have a more realistic synaptic drive, one may inject into the soma a current I_{dc}, which is a product of a Gauss-distributed conductance multiplied by a driving force that depends on the instantaneous membrane depolarization (Chance et al. 2002; Destexhe et al. 2001; Harsch and Robinson 2000)

$$I_{dc}(t) = \bar{g}_e x_e(t)(V_e - V(t)) + \bar{g}_i x_i(t)(V_i - V(t)) \quad \text{(A1)}$$

where $\bar{g}_e$, $\bar{g}_i$ (nS) are the excitatory and inhibitory peak conductances, respectively; V_e and V_i are the reversal potentials for AMPA and $GABA_A$ receptors (70 and −10 mV, respectively); $x_{e,i}(t)$ are Gauss-distributed variables with average $\mu_{xe,xi}$, variance $\sigma^2_{xe,xi}$ and time correlation length of $\tau_x = 1$ ms for both. $x_{e,i}(t)$ can be thought of as the probability of ion channel openings (normalized from zero to $\bar{g}_{e,i}$) attributed to a large number of independent excitatory and inhibitory postsynaptic potentials, each characterized by a sharp rise and an exponential decay with a time constant τ_x. The current that then actually flows into the cell depends on the depolarization $V(t)$ as expressed in *Eq. A1* for I_{dc}. The average and the variance of the AMPA conductance drive are a function of the quadruplet of parameters $\{N_e f_e, \bar{g}_e, N_i f_i, \bar{g}_i\}$

$$\mu_{xe} = N_e f_e \tau_x \quad \sigma^2_{xe} = \tfrac{1}{2} N_e f_e \tau_x$$

Analogous formulas were used for the inhibitory input (see also METHODS).

In the case of conductance drive, what is relevant for exploring the collective behavior of a population of neurons is the relation between the output spike frequency and the quadruplet of parameters $\{N_e f_e, \bar{g}_e, N_i f_i, \bar{g}_i\}$. Each quadruplet defines a possible statistics of the input and the distribution of the current can be determined by running a simulation of a LIF neuron in which the instantaneous current is computed at each time step according to *Eq. A1*. Given the average $\tilde{m}$ and the SD $\tilde{s}_I$ of the input current I_{dc}, it is not usually possible to predict correctly the output spike frequency because: *1*) the distribution of the current is slightly distorted by the driving force, which depends on the depolarization and the Gaussian approximation is no longer valid; *2*) the temporal correlations introduced by the driving force change the temporal statistics of the input current in a way that depends on the neuronal activity (see, e.g., Tiesinga et al. 2000). This means that if one injects a Gaussian current characterized by $m_I = \tilde{m}_I$ and $s_I = \tilde{s}_I$, in general one would not get the same spike rate as one would in the full simulation with the conductance drive I_{dc}.

However, for each quadruplet $\{N_e f_e, \bar{g}_e, N_i f_i, \bar{g}_i\}$ it is possible to generate a Gaussian current characterized by a pair $\{m_I, s_I\}$ that, when injected into a neuron, produces the same spike frequency as in the case of the conductance drive. The mean m_I and the variance s_I^2 of that current are given by

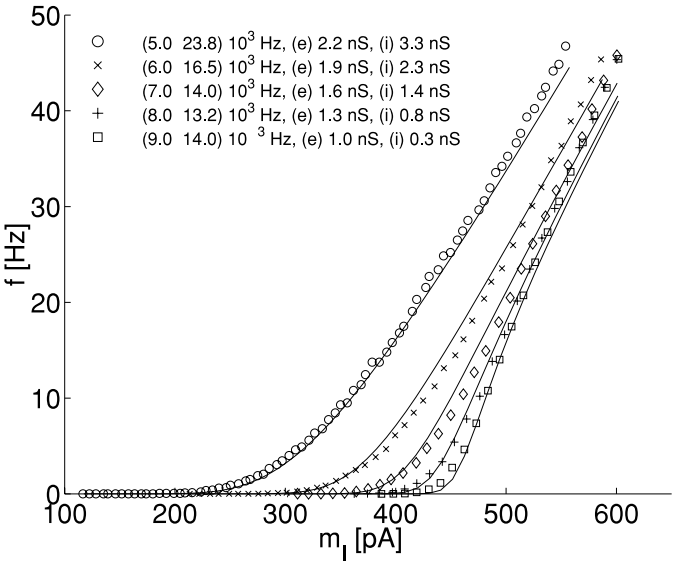

FIG. A1. Comparison between dynamic clamp (symbols) and current clamp (solid curves) driven LIF neuron after rescaling. Space of input currents determined by quadruplet $\{N_e f_e, \bar{g}_e, N_i f_i, \bar{g}_i\}$ is explored as explained in APPENDIX, and for each input current mean spike frequency is plotted. Each curve is generated by setting $g_{e,i}$ to values reported in *top left* of plot (nS), and then by sweeping along diagonal of $\{N_e f_e, N_i f_i\}$ plane. Ranges for $N_e f_e$ for each curve are different and are reported in figure (Hz). For each quadruplet mean current m_I is computed according to *Eq. A2* and reported on *bottom axis*. There are only small discrepancies between solid curves (current clamp) and corresponding symbols (dynamic clamp). Lifetime of simulation was 200 s; a transient of $4\tau_m = 80$ ms was discarded to allow current to reach its stationary behavior

$$m_I = \bar{g}_e N_e f_e \tau_I V_{E,\text{eff}} - \bar{g}_i N_i f_i \tau_I V_{I,\text{eff}} \quad \text{(A2)}$$

$$s_I^2 = \tfrac{1}{2}\, \bar{g}_e^2 N_e f_e \tau_I U^2_{E,\text{eff}} + \tfrac{1}{2}\, \bar{g}_i^2 N_i f_i \tau_I U^2_{I,\text{eff}}$$

where $V_{E,I,\text{eff}}$ and $U^2_{E,I,eff}$ are four positive scaling parameters in units of mV and mV^2, respectively, which do *not* depend on the statistics of the current determined by $\{N_e f_e, \bar{g}_e, N_i f_i, \bar{g}_i\}$, but only on the parameters that characterize the neuronal dynamics. This means that the scaling factors are unique for a wide range of inputs and that it is possible to predict the spike frequency in the case of a conductance drive for each quadruplet $\{N_e f_e, \bar{g}_e, N_i f_i, \bar{g}_i\}$. The recipe is simple: given the quadruplet one can determine m_I and s_I according to *Eq. A2* and then use the response function measured in the experiment to determine the output firing rate.

To prove that this is possible for a wide range of input currents we explored extensively the space of quadruplets $\{N_e f_e, \bar{g}_e, N_i f_i, \bar{g}_i\}$ and compared the output spike frequency in case of conductance drive and in case of current drive for the same simulated neuron. The neuron's parameters were: $\tau_r = 0$, $C = 500$ pF, $\theta = 20$ mV, $V_r = 10$ mV, $\tau = 20$ ms, $\alpha = 0$, and resting potential $V_{\text{rest}} = 0$. Our strategy to explore the input space was to keep constant $\bar{g}_{e,i}$ (nS) on each curve in Fig. A1 [values reported in the plot; the values for the *rightmost curve* correspond roughly to those used for AMPA and $GABA_A$ conductances in Harsch and Robinson (2000)], and then sweeping along the diagonal of the $\{N_e f_e, N_i f_i\}$ plane (i.e., $N_e f_e = N_i f_i$, frequency ranges reported in the plot). For each quadruplet $\{N_e f_e, \bar{g}_e, N_i f_i, \bar{g}_i\}$ we computed the spike frequency in the case of conductance drive [the simulated neuron was injected with $I_{dc}(t)$] and in the case of the injection of a Gaussian current with m_I, s_I given by *Eq. A2*. Note that s_I is not constant along each curve contrary to the plots shown in Fig. 6.

We show in Fig. A1 that it is possible to tune the four scaling parameters $V_{E,I,\text{eff}}$ and $U_{E,I,\text{eff}}$ in such a way that the neuron responds with the same mean spike frequency in the dynamic-clamp and in the current-clamp modalities. The unique scaling factors for all the inputs were: $V_{E,\text{eff}} = 51.1$ mV, $V_{I,\text{eff}} = 27.1$ mV, $U_{E,\text{eff}} = 24.7$ mV, and $U_{I,\text{eff}} = 30.2$ mV.

We are grateful to N. Buchs for having written the software for stimulation and data acquisition. We also thank T. Berger, N. Brunel, P. Del Giudice, A. Destexhe, W. Gerstner, and M. Mattia for stimulating discussions and for many useful remarks on the manuscript and G. Silberberg for helpful discussions about the experimental methods.

DISCLOSURES

This study was supported by Swiss National Science Foundation Grants 31-61335.00 and 3152-065234.01 and by Silva Casa Foundation.

REFERENCES

Abeles M. *Corticonics.* New York: Cambridge Univ Press, 1991.

Amit DJ and Brunel N. Model of global spontaneous activity and local structured (learned) delay activity during delay. *Cereb Cortex* 7: 237–252, 1997.

Amit DJ and Tsodyks MV. Quantitative study of attractor neural network retrieving at low spike rates I, substrate-spikes, rates and neuronal gain. *Network* 2: 259, 1991.

Amit DJ and Tsodyks MV. Effective neurons and attractor neural networks in cortical environment. *Network* 3: 121–137, 1992.

Brunel N. Dynamics of sparsely connected networks of excitatory and inhibitory spiking neurons. *J Comput Neurosci* 8: 183–208, 2000a.

Brunel N. Persistent activity and the single cell f–I curve in a cortical network model. *Network* 11: 261–280, 2000b.

Brunel N and Sergi S. Firing frequency of leaky integrate-and-fire neurons with synaptic currents dynamic. *J Theor Biol* 195: 87–95, 1998.

Brunel N and Wang X-J. Effects of neuromodulation in a cortical network model of object working memory dominated by recurrent inhibition. *J Comput Neurosci* 11: 63–85, 2001.

Chance FS, Abbott LF, and Reyes AD. Gain modulation from background synaptic input. *Neuron* 35: 773–782, 2002.

Cox DR and Miller HD. *The Theory of Stochastic Processes.* New York: Chapman & Hall, 1965.

Destexhe A and Paré D. Impact of network activity on the integrative properties of neocortical pyramidal neurons in vivo. *J Neurophysiol* 81: 1531–1547, 1999.

Destexhe A and Paré D. A combined computational and intracellular study of correlated synaptic bombardment in neocortical pyramidal neurons in vivo. *Neurocomputing* 32: 113–119, 2000.

Destexhe A, Rudolph M, Fellous JM, and Sejnowski TJ. Fluctuating dynamic conductances recreate in-vivo like activity in neocortical neurons. *Neuroscience* 107: 13–24, 2001.

Ermentrout B. Linearization of f–I curves by adaptation. *Neural Comput* 10: 1721–1729, 1998.

Fleidervish I, Friedman A, and Gutnick MJ. Slow inactiavation of current and slow cumulative spike adaptation in mouse and guinea-pig neocortical neurones in slices. *J Physiol* 493: 83–97, 1996.

Fourcaud N and Brunel N. Dynamics of the firing probability of noisy integrate-and-fire neurons. *Neural Comput* 14: 2057–2110, 2002.

Fuhrmann G, Markram H, and Tsodyks M. Spike frequency adaptation and neocortical rhythms. *J Neurophysiol* 88: 761–770, 2002.

Fusi S and Mattia M. Collective behavior of networks with linear (VLSI) integrate and fire neurons. *Neural Comput* 11: 633–652, 1999.

Fuster JM. *Memory in the Cerebral Cortex.* Cambridge, MA: MIT Press, 1995.

Gerstein GL and Mandelbrot B. Random walk models for the spike activity of a single neuron. *Biophys J* 4: 41–68, 1964.

Gerstner W and Kistler W. *Spiking Neuron Models: Single Neurons, Populations, Plasticity.* United Kingdom: Cambridge University Press, 2002.

Harsch A and Robinson HPC. Postsynaptic variability of firing in rat cortical neurons: the roles of input synchronization and synaptic NMDA receptor conductance. *J Neurosci* 20: 6181–6192, 2000.

Hsu SM, Raine L, and Fanger H. The use of avidin-biotin-peroxidase (ABC) in immunoperoxidase techniques: a comparison between ABC and unlabelled antibody (peroxidase) procedures. *J Histochem Cytochem* 29: 577–590, 1981.

Iansek R and Redman SJ. An analysis of the cable properties of spinal motoneurones using a brief intracellular current pulse. *J Physiol* 234: 613–636, 1973.

Kistler W, Gerstner W, and van Hemmen JL. Reduction of Hodgkin–Huxley equations to a threshold model. *Neural Comput* 9: 1069–1100, 1997.

La Camera G, Rauch A, Senn W, Luescher H-R, and Fusi S. Firing rate adaptation without losing sensitivity to input fluctuations. In: *Proceedings of ICANN2002,* edited by Dorronsoro JR. Heidelberg: Springer-Verlag, 2002, p. 180–185.

Larkum ME, Zhu JJ, and Sakmann B. A new cellular mechanism for coupling inputs arriving at different cortical layers. *Nature* 398: 338–341, 1999.

Liu Y-H and Wang X-J. Spike-frequency adaptation of a generalized leaky integrate-and-fire model neuron. *J Comput Neurosci* 10, 25–45, 2001.

Mainen ZF and Sejnowski T. Reliability of spike timing in neocortical neurons. *Science* 268: 1503, 1995.

Mainen ZF and Sejnowski TJ. Influence of dendritic structure on firing pattern in model neocortical neurons. *Nature* 382: 363–366, 1996.

Mattia M and Del Giudice P. Population dynamics of interacting spiking neurons. *Phys Rev E* 66: 051917, 2002.

McCormick DA, Connors BW, Lighthall JW, and Prince D. Comparative electrophysiology of pyramidal and sparsely stellate neurons of the neocortex. *J Neurophysiol* 54: 782–806, 1985.

Meyer PL. *Introductory Probability and Statistical Applications.* Reading, MA: Addison Wesley, 1965, p. 287.

Paré D, Shink E, Gaudreau H, Destexhe A, and Lang EJ. Impact of spontaneous synaptic activity on the resting properties of cat neocortical pyramidal neurons in vivo. *J Neurophysiol* 11: 1450–1460, 1998.

Powers RK, Sawczuk A, Musick JR, and Binder MD. Multiple mechanisms of spike-frequency adaptation in motoneurones. *J Physiol (Paris)* 93: 101–114, 1999.

Press W, Teukolsky SA, Vetterling WT, and Flannery BP. *Numerical Recipes in C: The Art of Scientific Computing.* United Kingdom: Cambridge University Press, 1992.

Rhodes P. Functional implications of active currents in the dendrites of pyramidal neurons. In: *Cerebral Cortex,* edited by Ulinski P, Jones EG, and Peters A. New York: Plenum Press, 1999, vol. 13.

Ricciardi LM. *Diffusion Processes and Related Topics in Biology.* Berlin: Springer-Verlag, 1977.

Rudolph M and Destexhe A. Correlation detection and resonance in neural systems with distributed noise sources. *Phys Rev Lett* 16: 3662–3665, 2001.

Sah P. Ca-activated K currents in neurons: types, physiological roles and modulation. *Trends Neurosci* 19: 150–154, 1996.

Salinas E and Sejnowski TJ. Integrate-and-fire neurons driven by correlated stochastic input. *Neural Comput* 14: 2111–2155, 2002.

Sanchez-Vives MV, Nowak LG, and McCormick DA. Cellular mechanisms of long-lasting adaptation in visual cortical neurons *in vitro. J Neurosci* 20: 4286–4299, 2000.

Sawczuk A, Powers RK, and Binder MD. Contribution of outward currents to spike frequency adaptation in hypoglossal motoneurons of the rat. *J Physiol* 78: 2246–2253, 1997.

Schwindt P, O'Brien JA, and Crill W. Quantitative analysis of firing properties of pyramidal neurons from layer 5 of rat sensorimotor cortex. *J Neurophysiol* 77: 2484–2498, 1997.

Schwindt PC, Spain WJ, and Crill WE. Long-lasting reduction of excitability by a sodium-dependent potassium current in cat neocortical neurons. *J Neurophysiol* 61: 233–244, 1989.

Smith PD, Liesegang RL, Berger RL, Czerlinski G, and Podolski RJ. A stopped-flow investigation of calcium ion binding by ethylene glycol bis-(beta-aminoethyl ether)-*N,N′*-tetraacetic acid. *Anal Biochem* 143: 188–195, 1984.

Tiesinga PHE, Jose JV, and Sejnowski TJ. Comparison of current-driven and conductance-driven neocortical model neurons with Hodgkin–Huxley voltage gated channels. *Phys Rev E* 62: 8413, 2000.

Traub RD and Miles R. *Neuronal Networks of the Hippocampus.* New York: Cambridge University Press, 1991.

Tsodyks M, Pawelzik K, and Markram H. Neural networks with dynamic synapses. *Neural Comput* 10: 821–835, 1998.

Tuckwell HC. *Introduction to Theoretical Neurobiology.* Massachusetts: Cambridge University Press, 1988.

Wang XJ. Calcium coding and adaptive temporal computation in cortical pyramidal neurons. *J Neurophys* 79: 1549–1566, 1998.

Wang XJ. Synaptic reverberation underlying mnemonic persistent activity. *Trends Neurosci* 24:455–463, 2001.

Yakovlev V, Fusi S, Berman E, and Zohary E. Inter-trial neuronal activity in infero-temporal cortex: a putative vehicle to generate long term associations. *Nat Neurosci* 1: 310–317, 1998.

Zhang L, Weiner JL, Valiante TA, Velumian AA, Watson PL, Jahromi SS, Schertzer S, Pennefather P, and Carlen PL. Whole-cell recording of the Ca-dependent slow afterhyperpolarization in hippocampal neurones: effects of internally applied anions. *Eur J Physiol* 426: 247–253, 1994.